

PACS numbers: 42.30.Wb; 87.63.L –; 87.64.Cc
DOI: 10.1070/QE2008v038n06ABEH013849

Method for remote diagnostics of the internal structure of layered media

V.V. Lychagov, A.L. Kalyanov, D.V. Lyakin, V.P. Ryabukho

Abstract. **The method of autocorrelation low coherence interferometry is proposed for diagnostics of inhomogeneities and the internal structure of layered technical and biological samples. In this method the low coherence optical field reflected from the layered sample is analysed by using a Michelson interferometer. Because the object is outside the interferometer, the distance between the interferometer and the object under study is not limited and thus the object can move during the measurements. Theoretical substantiation of the autocorrelation method for media with discrete and continuous optical structure modifications is presented.**

Keywords: *coherence, low-coherence interferometry, optical coherence tomography, biomedical diagnostics, layered sample*.

1. Introduction

Noninvasive methods for biological tissue investigation and inner structure visualisation open up wide possibilities for early diagnostics of a number of diseases. Low-coherence interferometry (LCI) and optical coherence tomography (OCT) are now the most promising and rapidly developing methods, which enable *in situ* reconstruction of optical inhomogeneities of biological tissues in real time with a high spatial resolution [1 – 7]. The present methods are based on the use of limited coherent properties of the applied light sources. The short temporal coherence length of the source determines the spatial resolution of the mentioned methods.

LCI and OCT are widely used in such fields as gastroenterology, urology, otolaryngology and cardiovascular disaster diagnostics. The OCT-based techniques are mainly used in ophthalmology because of the relative transparency of eye tissues. Nevertheless, despite the wide spread and well developed theoretical basis, there are still some unsolved problems, which make the further development of these methods difficult.

V.V. Lychagov, A.L. Kalyanov, V.P. Ryabukho N.G. Chernyshevsky Saratov State University, ul Astrakhanskaya 83, 410012 Saratov, Russia; e-mail: lychagov@optics.sgu.ru;
D.V. Lyakin Institute for Problems of Precise Mechanics and Control, Russian Academy of Sciences, ul. Rabochaya 24, 410028 Saratov, Russia

Received 27 December 2007; revision received 13 March 2008
Kvantovaya Elektronika **38** (6) 563 – 569 (2008)
Translated by V.V. Lychagov

In conventional LCI and OCT methods the object is located in one of the arms of the dual beam interferometer (typically Michelson interferometer) at which output the interference of two beams is observed – the first one is the reference beam and the second one is the sample beam reflected from the object under study [1, 2, 5, 6]. This implementation imposes limitations on the distance between the object and interferometer. Moreover, it is difficult to control moving and unstable objects. These conditions limit greatly the application of the conventional LCI method in clinical and *in vivo* studies when an object should be isolated from the measuring part of the interferometric scheme and the system should have a high noise stability and low sensitivity to the accidentally changing properties of the object.

The problems related to the limitation of the distance between the interferometer and the object and the displacements of the object during its control can appear in different modifications of LCI with a reference beam, including recently developed phase modulated LCI [8 – 10]. Similar problems take place in spectral LCI where the reference beam is used. In spectral LCI with a broadband source [2, 4, 7, 11 – 17], the limitation on the optical path difference in the sample and reference arms of the interferometer is caused by the finite spectral resolution of the spectral system [7, 16, 17]. Because the period of interference oscillations in the spectrum is inversely proportional to the optical path difference, if the path difference in the spectral system is too large, oscillations cannot be resolvable either by the spectrograph or the linear detector array used for light detection. In swept laser source LCI [4, 7, 16 – 23], the limitation on the maximum optical path difference is caused by the finite bandwidth of the source and related accuracy of the sweeping. When the optical path difference is large, the bandwidth of the source should be sufficiently narrow and, as a result, spectral tuning should be more precise.

There are two similar LCI and OCT methods that overcome these limitations. In the so-called dual beam LCI, the controlled object is located outside the interferometer and is illuminated by a low coherence light field formed at the interferometer output [3, 4, 24, 25]. In this method the controlled object is located between the interferometer and the photodetector, and the interferometer in this case is a light source forming a light beam with controlled longitudinal coherence features.

One more LCI method without a reference beam is proposed in [26] where the object under study, unlike the dual beam LCI method, is between a light source and a detector. In this method the light beam reflected from the

layered object (film) is directed to the Michelson interferometer where the optical path difference between the waves reflected from different layers within the sample is compensated for and white light interference fringes are observed. In this method, as in the dual beam LCI, the object under study is outside the interferometer and a special reference beam is not used. Thus, theoretically the distance to the object can be arbitrary and axial movements of the object almost do not affect the parameters of the interferometric signal.

This implementation of LCI despite its practical merits has not been developed in theory and practice, including the OCT methods. Besides its practical advantages, this LCI method attracts attention from the theoretical point of view and due to features of the interferometric signal formation. This work is aimed at the development of the theoretical concepts underlying the LCI method being discussed.

2. Low coherence autocorrelation interferometry theory

Suppose that the coherence length $l_c \approx c2\pi/\Delta\omega$ of the incident field $E_0(z,t)$ is sufficiently short. Here $\Delta\omega$ is the spectrum bandwidth [27, 28]. In this method just as in standard LCI the coherence length l_c determines in-depth resolution of the system. Therefore, optical thicknesses of layers within the sample under study should be either comparable with or more than the coherence length of the source.

To simplify the analysis of the interferometric signal formation a collimated incident field and a collimated sample field are considered. In other words, we assume that optical fields have narrow angular spectra and the influence of the angular spectrum on the autocorrelation signal can be neglected [29].

The total object field of thickness d is a superposition of elementary fields reflected from boundaries within the layered sample. The optical field reflected from the border of an elementary layer dz' located at the depth z' (Fig. 1) can be written in the form

$$dE_S(z,t) = \rho(z')\exp\left(-2\int_0^{z'}\mu_T(\tilde{z})d\tilde{z}\right) \times E_0\left(z, t-\frac{2nz'}{c}\right)dz', \quad (1)$$

where z is traveling direction of the sample field; $\rho(z')$ is the amplitude reflection of the media at the depth z'; $\mu_T(\tilde{z})$ is the amplitude collimated transmittance of the $d\tilde{z}$-thick layer at the depth $\tilde{z}$; n is the mean refractive index of the medium inside the object. The term $\Delta t' = 2nz'/c$ shows the time delay of the oscillations reflected from an elementary layer dz' at the depth z' within the object.

Let the new coefficient $R(z')$ involve reflection and transmittance and characterise optical properties of the object along the depth of light penetration:

$$R(z') = \rho(z')\exp\left(-2\int_0^{z'}\mu_T(\tilde{z})d\tilde{z}\right). \quad (2)$$

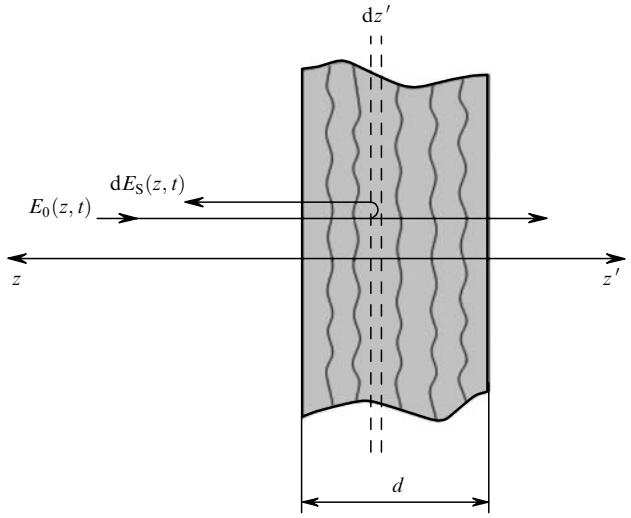

Figure 1. Formation of an optical field reflected from a bulky scattering layered sample.

The total sample field $E_S(z,t)$ reflected from the whole of the object is a superposition of fields (1):

$$E_S(z,t) = \int_0^d R(z')E_0\left(z, t-\frac{2nz'}{c}\right)dz'. \quad (3)$$

The field (3) is directed to the interferometer the variable part of the output autocorrelation signal of which can be written in the form:

$$\begin{aligned}\tilde{I}(\Delta t) &= 2\mathrm{Re}\langle E_S(t)E_S^*(t-\Delta t)\rangle \\ &= 2\mathrm{Re}\left\langle\int_0^d R(z')E_0\left(z, t-\frac{2nz'}{c}\right)dz'\int_0^d R^*(z'')\right. \\ &\left.\times E_0^*\left(z, t-\frac{2nz''}{c}-\frac{2\Delta z_m}{c}\right)dz''\right\rangle \quad (4)\\ &= 2\mathrm{Re}\int_0^d\int_0^d R(z')R^*(z'')\left\langle E_0\left(z, t-\frac{2nz'}{c}\right)\right. \\ &\left.\times E_0^*\left(z, t-\frac{2nz''}{c}-\frac{2\Delta z_m}{c}\right)\right\rangle dz'dz''.\end{aligned}$$

It can be rewritten depending on the optical path difference $2\Delta z_m$ determined by the difference in the positions of two mirrors in the interferometer $2\Delta z_m = \Delta tc$:

$$\tilde{I}(2\Delta z_m) = 2\mathrm{Re}\int_0^d\int_0^d R\left(z'+\frac{\Delta z'}{2}\right)R^*\left(z'-\frac{\Delta z'}{2}\right) \times \Gamma(2n\Delta z' - 2\Delta z_m)dz'd\Delta z', \quad (5)$$

where variables $\hat{z} = (z' - z'')/2$, $\Delta z' = z' - z''$, $\hat{z} \to z'$ were replaced; $\Gamma(\Delta) = \langle E_0(z,t)E_0^*(z,t-\Delta/c)\rangle$ is the complex temporal coherence function of the incident field; Δ is the optical path difference. In Eqn (5) for the output signal of the interferometer, the integral

$$B(\Delta z') = \int_0^d R\left(z' + \frac{\Delta z'}{2}\right) R^*\left(z' - \frac{\Delta z'}{2}\right) \mathrm{d}z' \tag{6}$$

defines the autocorrelation function of the in-depth (axial) optical structure of the object.

Expression (5) is a convolution of the correlation function $B(\Delta z')$ of the optical structure of the object and the coherence function $\Gamma(\Delta z')$ of the incident field. When probe broadband radiation ($G(\omega) = G_0 = \text{const}$ is the white light) is used and l_c is shorter than the mean wavelength, the coherence function can be assumed to be the δ-function: $\Gamma(2n\Delta z' - 2\Delta z_m) = I_0\delta(2n\Delta z' - 2\Delta z_m)$. Applying this for Eqn (5) and using the filtering property of the δ-function we obtain the expression for the interference signal:

$$\tilde{I}(2\Delta z_m) \sim B\left(\frac{2\Delta z_m}{2n}\right), \tag{7}$$

assuming that $B(\Delta z')$ is a real function. In this case, the interference signal consists of only one oscillation.

If the coherence length of incident radiation is finite, Eqn (5) can be written in the form:

$$\tilde{I}(2\Delta z_m) \sim \int_0^d B(\Delta z')|\Gamma(2n\Delta z' - 2\Delta z_m)| \times \cos(\kappa 2n\Delta z' - \kappa 2\Delta z_m)\mathrm{d}\Delta z'. \tag{8}$$

There are some interference oscillations with a period equal to the average wavelength $\lambda = 2\pi/\kappa$ in the signal represented by the optical path difference $2\Delta z_m$.

Because the interference signal envelope is informative and Eqn (8) has a maximum when $\cos(\kappa 2n\Delta z' - \kappa 2\Delta z_m) = \pm 1$, the multiplier $\cos(\kappa 2\Delta z_m)$ can be factored out:

$$\tilde{I}(2\Delta z_m) \sim \left\{\int_0^d B(\Delta z')|\Gamma(2n\Delta z' - 2\Delta z_m)|\,\mathrm{d}\Delta z'\right\} \times \cos(\kappa 2\Delta z_m). \tag{9}$$

The multiplier $\cos(\kappa 2\Delta z_m)$ in Eqn (9) determines high frequency carrier oscillations in the interference signal. Detection of this signal (demodulation) leads to the expression for the interferometric output signal:

$$\tilde{I}(2\Delta z_m) \sim \int_0^d B(\Delta z')|\Gamma(2n\Delta z' - 2\Delta z_m)|\mathrm{d}\Delta z'. \tag{10}$$

This expression can be used to interpret the results of measurements carried out with the interferometric method being considered. In particular, the spatial spectrum of the object structure can be written in the form:

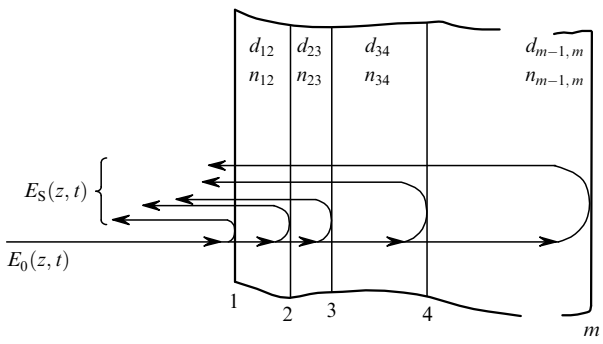

Figure 2. Formation of an optical field reflected from the sample consisting of transparent layers with sharp boundaries.

$$F\{B(\Delta z')\} = \frac{F\{\tilde{I}(2\Delta z_m)\}}{F\{|\Gamma(2\Delta z_m)|\}}, \tag{11}$$

where $F\{\}$ is a Fourier transform.

Consider the case when the object consists of $m-1$ transparent layers delimited with m thin reflecting boundaries (Fig. 2). Then, the complex reflectances of these boundaries are $\rho_1 = \rho_{01}\exp(\mathrm{i}\varphi_1)$, $\rho_2 = \rho_{02}\exp(\mathrm{i}\varphi_2), \ldots,$ $\rho_m = \rho_{0m}\exp(\mathrm{i}\varphi_m)$.

We do not take into account a multiple reflection within the layers. In this case, the electric field intensity of the total sample field $E_S(z,t)$ propagating along the z axis is:

$$E_S(z,t) = \sum_{j=1}^{m} R_j E_0(z, t - \Delta t_{1j}), \tag{12}$$

where $E_0(z,t) = U_0(z,t)\exp(\mathrm{i}\omega_0 t)$ is the wave disturbance of the incident field; j is a reflecting boundary number; Δt_{1j} is the mutual time delay between wave disturbances reflected from the first and jth boundaries; ω_0 is the central cyclic frequency of the field; $R_j = \rho_j\prod_{k=1}^{j-1}(1-\rho_{0k})^2$ are the complex indices taking into account the object reflection properties of the layer boundaries.

The total sample field $E_S(z,t)$ is directed into the scanning Michelson interferometer with flat mirrors, one of them moving under control along the optical axis. The variable part $\tilde{I}(2\Delta z_m)$ of the output signal will have the form:

$$\tilde{I}(2\Delta z_m) = 2\sum_{j=1}^{m}|R_j|^2|\Gamma(2\Delta z_m)|\cos(\kappa_0 2\Delta z_m) \times \sum_{i=1}^{m-1}\sum_{j=i+1}^{m}|R_i R_j^*|\left|\Gamma\left(2\Delta z_m \pm \sum_{k=i}^{j-1}2d_{k,k+1}n_{k,k+1}\right)\right| \times \cos\left(\kappa_0 2\Delta z_m \pm \kappa_0\sum_{k=i}^{j-1}2d_{k,k+1}n_{k,k+1} + \varphi_i - \varphi_j\right), \tag{13}$$

where $\kappa_0 = 2\pi/\lambda_0 = \omega_0/c$; $\Delta t = 2\Delta z_m/c$; $\Delta t_{ij} = 2d_{ij}n_{ij}/c$; $d_{ij}n_{ij}$ is the optical thickness of the layer between the ith and jth boundaries. According to Eqn (13), the high-frequency interference signal is determined by the cosine multiplier $\cos(\kappa_0 2\Delta z_m)$ and is modulated with the coherence function $\Gamma(2\Delta z_m \pm \Delta_j)$, where Δ_j is the optical path

difference due to corresponding object layers and their combinations. The cosine multiplier $\cos(\kappa_0 2\Delta z)$ in Eqn (13) defining the carrier frequency of the signal can be factored out if the phase shifts $\kappa_0 2d_{ik}n_{ik}$ and $\varphi_i - \varphi_j$ (independent of Δz_m) are neglected.

Expression (13) shows that the variable part $\tilde{I}(2\Delta z_m)$ of the output signal of the interferometer consists of several interference peaks of temporal coherence when the optical path difference in the interferometer changes according to $\Delta = \pm 2\Delta z_m$. The position of these pulses is determined by the equality of the argument of the coherence function $\Gamma(\Delta)$ to zero, because $\Gamma(\Delta = 0) = I_0$. The central peak observed for $2\Delta z_m = 0$ (the first term in the equation) is related to the zero optical path difference in the interferometer. It contains no information about the axial structure of the sample field and, therefore, about the inner structure of the object.

The side pulses are located symmetrically with respect to the central peak. The position of these side pulses in the interference signal is determined by optical thicknesses of layers and theirs combinations within the sample. They are given by the second term in the argument of the function $\Gamma(\Delta)$ in the second term of Eqn (13). One can easily determine from Eqn (13) that the total number N of side peaks in the autocorrelation LCI signal is:

$$N = \frac{1}{2}(m^2 - m). \tag{14}$$

Note that the autocorrelation signal has peaks corresponding to the combinations of consecutive layers only.

3. Experimental results

The experimental setup was based on a Michelson interferometer (Fig. 3) with a mirror operating at a frequency of $f_0 \approx 1$ Hz with the amplitude $l_0 \approx 1$ mm. This scanning amplitude is significantly larger than the optical thickness of the whole of the object. Two cover glasses of different thicknesses were used as a layered object. The surface of one of them was covered with 20-nm thick gold nanoshells deposited on SiO_2 cores of diameter 180 nm. The choice of the object was caused by the availability of using nanoobjects for the contrast enhancement in low coherence interferometry and tomography [30, 31]. Besides, another object was studied, which consisted of two glasses – cover glass and slide plate. The slide plate was covered with a 4–5-μm thick skin abruption.

A superluminescent diode SLD emitting at the central wavelength $\lambda_{SLD} = 850$ nm was used as a light source. In-depth scanning of the object was realised with the help of the continuous axial displacement of the mirror M2 within the Michelson interferometer MI. To determine the displacement of the mirror M2, an auxiliary laser channel was used in the interferometer, which formed, upon moving the mirror M2, a 'laser scale' with a resolution determined by the fractions of the LD central wavelength $\lambda_{LD} =$ 650 nm. Lateral scanning is performed by using a controllable motorised translation stage with a 50-μm resolution. The sample signal $u_S(2\Delta z_m)$ and laser signal $u_R(2\Delta z_m)$ were recorded and digitised simultaneously for further processing.

The images obtained with the use of the autocorrelation LCI system are presented in Figs 4c, d. The relative position

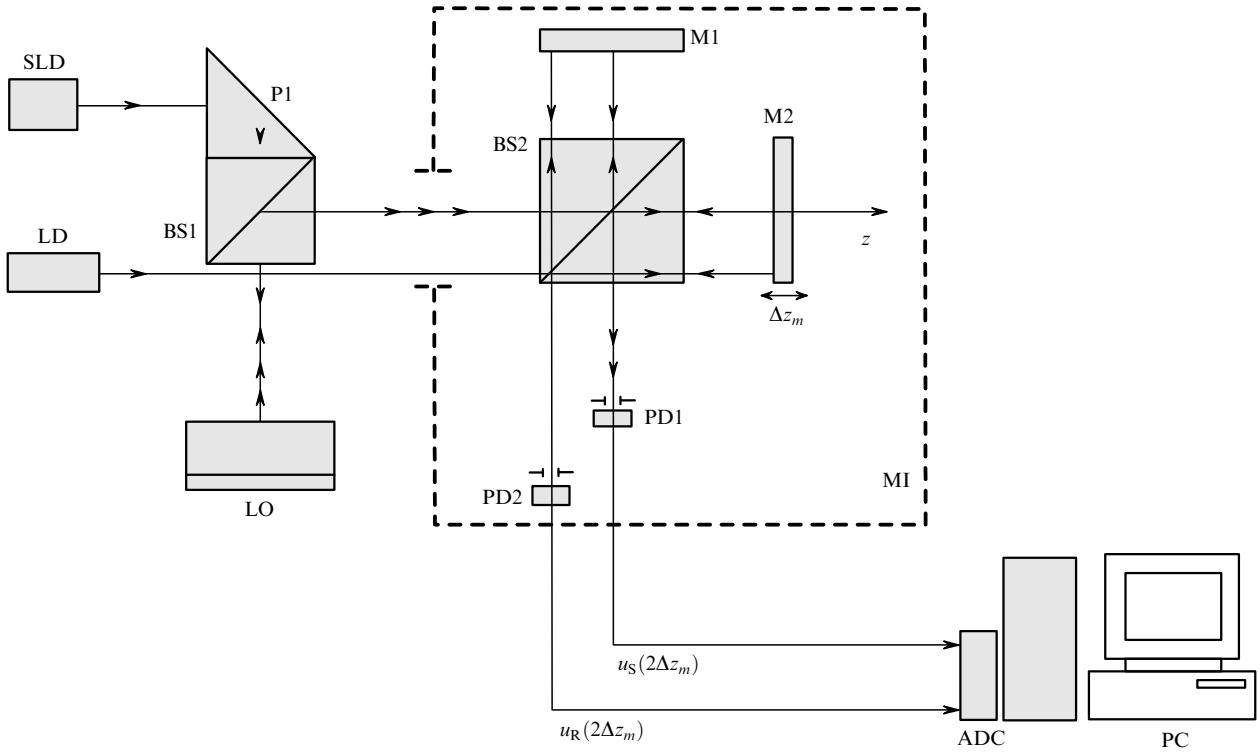

Figure 3. Autocorrelation low-coherence interferometry setup: SLD – superluminescent diode; P1 – right angle prism; BS1, BS2 – beamsplitters; LO – layered object; M1, M2 – mirrors; LD – laser diode; PD1, PD2 – photodiodes; MI – Michelson interferometer; $u_S(2\Delta z_m)$ – autocorrelation interference signal; $u_R(2\Delta z_m)$ – laser interference signal; ADC – analog-to-digital converter.

of the object with respect to the light propagation direction is shown in Figs 4a, b. It is significant that these images depict not the object inner structure but the spatial scan of the modulus of the sample field autocorrelation function. Thus, this image is a cross-section autocorrelation image of the object inner structure.

It is possible to reconstruct the optical structure of the object by using these images. The first side signal at the 50-μm level (Fig. 4c) is related to the thinnest layer of the object – it is an air gap of thickness 25 μm. The next signal at the 440-μm level refers to thinnest cover glass (*2*) coated with gold nanoshells. The thickness of this layer calculated from the signal geometry is 147 μm. The following signal at the 490-μm level is related to the combination of two layers – thin cover glass (*2*) and the air gap. The signal at the 800-μm level corresponds to cover glass (*1*). Its calculated geometrical thickness is 267 μm. The next signal at the 840-μm level corresponds to the combination of cover glass (*1*) and the air gap. The last signal at the 1280-μm level refers to the combination of optical thicknesses of all three layers of the object. In Fig. 4c the edge of the layer of nanoparticles is well observed and the influence of nanoshells on the interference signal can be estimated. The changes are mainly observed in the signal, which is the result of interference of two waves, one of them passing through the nanoshell layer, and the other being reflected from it. In our case, this is the signal corresponding to cover glass (*2*). In addition, signals formed by only one wave, which either passed through the nanoshell layer or was reflected from it, experience significant changes.

In Fig. 4d the first side signal at the 320-μm level is related to the 105-μm thick cover glass. The second signal may be related to the air gap of variable thickness, at a certain point the optical thickness of the air gap becoming equal to the optical thickness of the cover glass. The third interference signal is related to the sum of the air gap and the cover glass optical thicknesses (Fig. 4b). Note that the wave, which appears due to diffuse reflectance of the skin abruption pasted on the slide plate, produces the second and third interference pulses. This experiment shows the potential of the autocorrelation low-coherence interferometry for diagnostics of highly scattering media including biological tissues.

4. Conclusions

In conventional low coherence interferometry with a reference beam, temporal coherence pulses in the interference signal are referred to the optical depth of occurrence of layers within the sample.

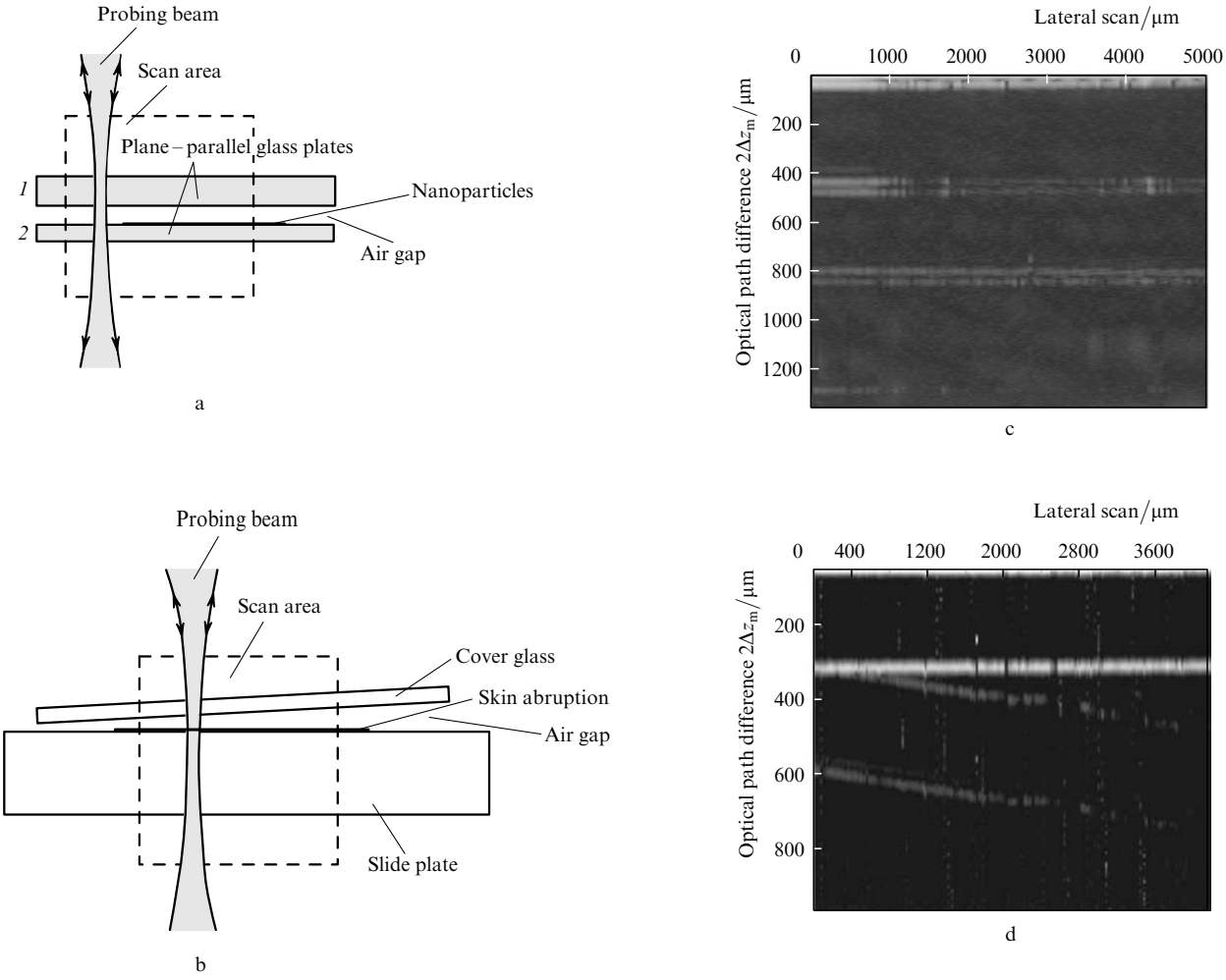

Figure 4. Cross sections of samples with nanoparticles (a) and with skin abruption (b) and autocorrelation interference signals corresponding to them (c, d).

In the system under study interference signals show relative positions of the reflecting boundaries [26]. The first peak refers not to the nearest but to the thinnest layer independent of its depth of occurrence. This property is both an advantage and disadvantage of the interference system. In the case when the object consists of only one layer (for example measurements of glasses, transparent coatings and films and single air gaps) this is an advantage. The interference pulse position in the signal points definitely to the required parameter – optical thickness of the layer. It is also suitable for diagnostics when *a priori* information about the sequence of reflecting boundaries is known, for example in ophthalmology especially to control the axial geometry of transparent eye tissues [4].

However, when the structure of the sample is unknown, the autocorrelation interference signal allows defining only thicknesses of layers but not their disposition. Moreover, if there are several layers with the same optical thicknesses within the sample, the interference pulses from them will coincide and they will be interpreted as one layer. In addition, the pulses can suppress one another if they are out-of-phase.

One more disadvantage is a low intensity of the signal because of the absence of the reference beam. In conventional LCI the signal increases due to heterodyne mixing with an intense reference beam.

However, the autocorrelation LCI system has a number of advantages over standard LCI [26]. First of all:

(i) The distance to the object is not limited. We can control remote objects with the help of autocorrelation LCI. It is important for a number of technical problems especially for working with a corrosive media and for biomedical *in vivo* research when close contact with the object is difficult.

(ii) The distance to the object under control may change during the measurements. Therefore, it is possible to control axially moving objects. The object time instability including vibrations does not affect the experimental results. It is very important for studying living objects.

(iii) The interferometer does not need complex maintenance.

(iv) We can use a free-space interferometer, which leads to the high optical efficiency of the method. It is possible to use an optical multimode fibre or even multiple fibres for illuminating the object and for collecting reflected light.

We suppose these properties allow using the autocorrelation low-coherence interferometry method in many research and diagnostics problems including biomedical diagnostics.

Acknowledgements. Authors thank N.G. Khlebtsov for preparing the sample with nanoshells and I.L. Maksimova for useful discussions of results. This research was supported by the Russian Foundation for Basic Research (Grant Nos 05-08-65514-a and 07-02-01434) and CRDF RUX0-006-SR-06 (ANNEX BP1M06).

References

1. Ivanov A.P., Chaikovski A.P., Kumeisha A.A. *Dokl. Akad. Nauk BSSR*, **23** (6), 503 (1979).
2. Huang D., Swanson E.A., Lin C.P., Schuman J.S., Stinson W.G., Chang W., Hee M.R., Flotte T., Gregory K., Puliafito C.A., Fujimoto J.G. *Science*, **254**, 1178 (1991).
3. Fercher A.F., Hitzenberger C.K., Drexler W. *Proc. SPIE Int. Soc. Opt. Eng.*, **2732**, 210 (1996).
4. Fercher A.F., Drexler W., Hitzenberger C.K., Lasser T. *Rep. Progr. Phys.*, **66**, 239 (2003).
5. Gelikonov V.M., Gelikonov G.V., Gladkova N.D., Kuranov R.V., Nikulin N.K., Petrova G.A., Pochinko V.V., Pravdenko K.I., Sergeeva A.M., Feldshtein F.I., Hanin Y.I., Shabanov D.V. *Pis'ma Zh. Tekhn. Fiz.*, **61** (2), 149 (1995).
6. Schmitt J.M. *IEEE J. Sel. Top. Quantum Electron.*, **5** (4), 1205 (1999).
7. Tomlins P.H., Wang R.K. *J. Phys. D: Appl. Phys.*, **38**, 2519 (2005).
8. Varghese B., Rajan V., van Leeuwen T.G., Steenbergen W. *Opt. Express*, **15** (20), 13340 (2007).
9. Varghese B., Rajan V., van Leeuwen T.G., Steenbergen W. *J. Biomed. Opt.*, **12**, 024020 (2007).
10. Varghese B., Rajan V., van Leeuwen T.G., Steenbergen W. *Opt. Express*, **15** (15), 9157 (2007).
11. Fercher A.F., Hitzenberger C.K., Kamp G., Elzaiat S.Y. *Opt. Commun.*, **117**, 43 (1995).
12. Morgner U., Drexler W., Kartner F.X., Li X.D., Pitris C., Ippen E.P., Fujimoto J.G. *Opt. Lett.*, **25**, 111 (2000).
13. Wojtkowski M., Leitgeb R., Kowalczyk A., Bajraszewski T., Fercher A.F. *J. Biomed. Opt.*, **7**, 457 (2002).
14. Wojtkowski M., Kowalczyk A., Leitgeb R., Fercher A.F. *Opt. Lett.*, **27** (16), 1415 (2002).
15. de Boer J.F., Cense B., Park B.H., Pierce M.C., Tearney G.J., Bouma B.E. *Opt. Lett.*, **28**, 2067 (2003).
16. Choma M.A., Sarunic M.V., Yang C., Izatt J.A. *Opt. Express*, **11** (18), 2183 (2003).
17. Sarunic M.V., Choma M.A., Yang C., Izatt J.A. *Opt. Express*, **13** (3), 957 (2005).
18. Chinn S.R., Swanson E.A., Fujimoto J.G. *Opt. Lett.*, **22**, 340 (1997).
19. Golubovic B., Bouma B.E., Tearney G.J., Fujimoto J.G. *Opt. Lett.*, **22**, 1704 (1997).
20. Lexer F., Hitzenberger C.K., Fercher A.F., Kulhavy M. *Appl. Opt.*, **36**, 6548 (1997).
21. Haberland U.H.P., Blazek V., Schmitt H.J. *J. Biomed. Opt.*, **3**, 259 (1998).
22. Choma M.A., Yang C., Izatt J.A. *Opt. Lett.*, **28**, 2162 (2003).
23. Choma M.A., Hsu K., Izatt J.A. *J. Biomed. Opt.*, **10** (4), 044009 (2005).
24. Ivanov V.V., Markelov V.A., Novikov M.A., Ustavchikov S.S. *Pis'ma Zh. Tekhn. Fiz.*, **30** (9), 82 (2004).

25. Kononenko V.V., Konov V.I., Pimenov S.M., Volkov P.V., Gorunov A.V., Ivanov V.V., Novikov M.A., Markelov V.A., Tertishnik A.D., Ustavchikov S.S. *Kvantovaya Elektron*., **35** (7), 622 (2005) [*Quantum Electron*., **35** (7), 622 (2005)].
26. Flournoy P.A., McClure R.W., Wyntjes G. *Appl. Opt*., **11** (9), 1907 (1972).
27. Born M., Wolf E. *Principles of Optics* (Oxford: Pergamon Press, 1970).
28. Mandel L., Wolf E. *Optical Coherence and Quantum Optics* (Cambridge: Cambridge University Press, 1995).
29. Ryabukho V.P., Lyakin D.I., Lychagov V.V. *Opt. Spektr*., **102** (6), 996 (2007).
30. Trouthman T.S., Barton J.K., Romanowski M. *Opt. Lett*., **32** (11), 1438 (2007).
31. Khlebtsov B.N., Khanadeyev V.A., Ye J., Mackowski D.W., Borghs G., Khlebtsov N.G. *Phys. Rev. B*, **77**, 035440 (2008).